ISSN: 2960-0103

DOI: https://doi.org/10.61784/wjmp3018

THERMAL EFFECTS IN A LD-END-PUMPED PR³⁺: YLF GREEN LASER

Bo Li*, JianSheng Zhang

Department of Physics, School of Basic Sciences, Xi'an Technological University, Xi'an 710021, Shaanxi, China. Corresponding Author: Bo Li, Email: 2630048895@qq.com

Abstract: This paper systematically investigates the thermal effects in a laser diode (LD) end-pumped Pr³⁺: YLF green laser. Through numerical simulation, the evolution of the internal temperature field under different pump powers (4-20 W) was analyzed. The results reveal that the heat source and temperature exhibit an exponential decay along the crystal axis, with a persistent hot spot at the pump end-face. Increasing the pump power significantly expands the high-temperature region and intensifies the spatial temperature gradient, leading to severe thermal lensing. Furthermore, the dependence of the thermal lens focal length on key parameters was quantified. The focal length decreases nonlinearly with increasing pump power and decreasing pump spot radius, while a larger crystal diameter alleviates the effect by improving heat dissipation. These findings provide critical insights for the thermal management and resonator design of high-power visible lasers.

Keywords: Pr³⁺: YLF laser; End-pumping; Thermal effect; Temperature field; Thermal lensing effect

1 INTRODUCTION

Among visible laser gain media, the Pr³⁺:YLF crystal has garnered considerable interest due to its abundant energy level transition characteristics. As an excellent laser gain medium, it exhibits rich spectral properties covering a broad range from blue to red light, with particularly outstanding emission characteristics in the green spectral region, making it an ideal material for achieving efficient green laser output.

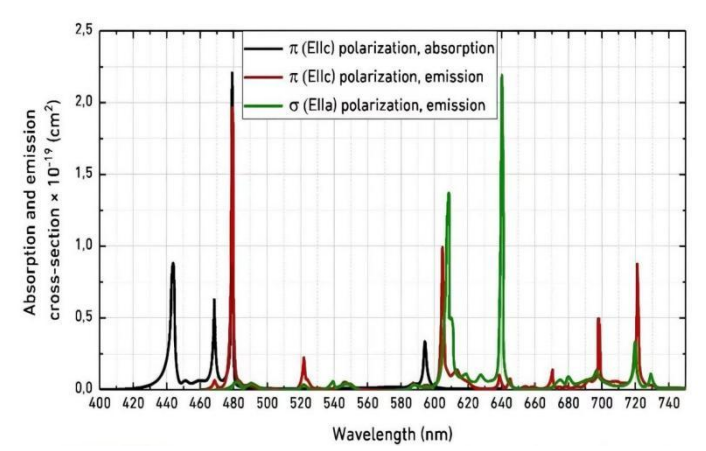


Figure 1 Absorption and Emission Spectra of Pr³⁺: YLF Crystal

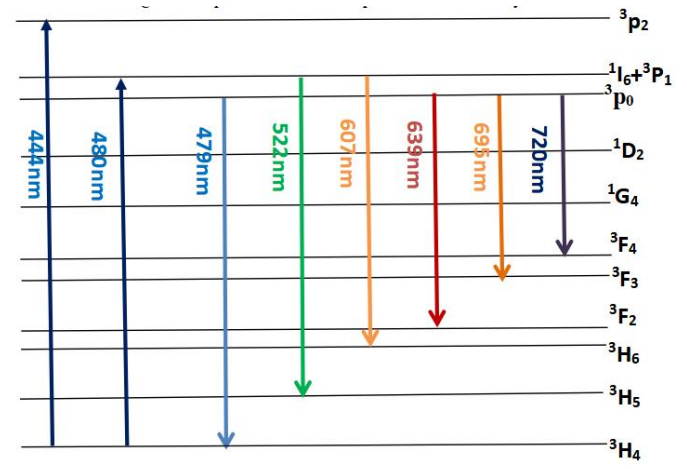


Figure 2 Energy Level Diagram of Pr³⁺ ions

As shown in the absorption and emission spectra in Figure 1, the crystal exhibits significant absorption peaks near 444 nm and 479 nm, providing an ideal spectral matching foundation for GaN-LD pumping. The corresponding energy level structure of Pr³⁺ ions is shown in Figure 2, and its multi-level characteristics support multiple laser transitions from blue to infrared light.

This study focuses on the 522 nm green laser characteristics of Pr³⁺:YLF crystals. While this transition has a relatively low emission cross-section, proper thermal management enables significant improvement in conversion efficiency. In the LD end-pumped configuration, strong pump absorption at the crystal end-face creates non-uniform heat deposition, forming radial temperature gradients that lead to thermal lensing effects and consequently affect laser performance and stability. Therefore, detailed investigation of thermal effects—particularly temperature field distribution and thermal lens properties—in end-pumped Pr³⁺:YLF crystals is crucial for developing high-power, stable green lasers[1-5]. Through thermal conduction modeling and rate equation analysis, this work establishes the relationship between pumping parameters and thermal effects, providing theoretical guidance for laser resonator design.

2 THEORETICAL MODELS AND METHODS

2.1 Four-Level Rate Equation Model

To analyze the output characteristics of the Pr³⁺: YLF laser, a steady-state rate equation model based on the four-level system is established[6-8]. The variation of the upper laser level population N₂ can be expressed as:

$$\frac{dN_2}{dt} = \frac{\eta_p P_p}{h v_p V} - \frac{N_2}{\tau} - \sigma_{em} N_2 \Phi \tag{1}$$

 η_p represents the pump absorption efficiency, p_p denotes the pump power, h_{V_p} represents the photon energy of the pump radiation, V denotes the effective mode volume, τ denotes the upper-level lifetime, σ_{em} denotes the stimulated emission cross-section, Φ denotes the photon flux density. Under steady-state conditions, $\frac{dN_2}{dt} = 0$, the population inversion is determined by the pump power and the upper-level lifetime. Under steady-state conditions $(\frac{dN_2}{dt} = 0)$, the population inversion density:

$$N_{2} = \frac{\eta_{p} P_{in}}{h v_{p} V \left(\frac{1}{\tau} + \sigma_{em} \Phi\right)}$$
 (2)

2.2 Thermal Lens Theory Model

In Pr³⁺:YLF crystals, a portion of the absorbed pump energy is converted to heat within the crystal bulk, establishing temperature gradients and refractive index variations that collectively give rise to thermal lensing effects. The radial temperature distribution in the crystal can be approximated as:

$$\Delta T(r) = \Delta T_0 \left(1 - \frac{r_b^2}{\omega_p^2} \right)$$
 (3)

where ΔT_0 represents the maximum temperature rise at the crystal center, ω_p denotes the pump beam radius, and the temperature-dependent refractive index variation follows:

$$n(r) = n_0 - \left(\frac{dn}{dT}\right) \Delta T(r) \tag{4}$$

Combining the stress-optic effect from thermal expansion, the crystal acts as a gradient-index medium with thermal lens focal length expressed as [9-12]:

$$f_{\rm th} = \frac{\pi k \omega_p^2}{P_{abs} \cdot (dn/dT)}$$
 (5)

3 ANALYSIS AND DISCUSSION

3.1 Evolution of Crystal Temperature Fields and Heat Sources

To systematically study thermal effects in LD end-pumped Pr³⁺: YLF crystals, this section numerically simulates the heat source distribution, axial temperature profile, and two-dimensional temperature field evolution under various pump powers.

These three sets of results corroborate each other, collectively revealing the formation mechanisms and spatial characteristics of the thermal effects.

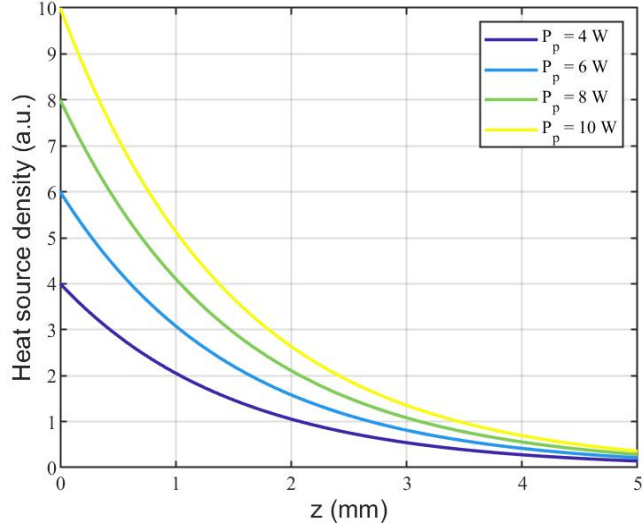


Figure 3 Axial Heat Source Distribution under Varied Pump Power

Figure 3 illustrates the heat source density distribution along the optical axis (Z-axis) of the crystal under different pump powers. It can be observed that the heat source density reaches its maximum at the pump incident end z=0 and exhibits an exponential decay trend with increasing penetration depth. This behavior is attributed to the strong absorption of pump photons by Pr^{3+} ions during propagation through the crystal. Furthermore, as the pump power increases from 4 W to 10 W, the overall heat source density within the crystal increases linearly while the spatial distribution profile remains essentially unchanged. This indicates that the pump power primarily influences the magnitude of heat generation rather than altering the distribution pattern.

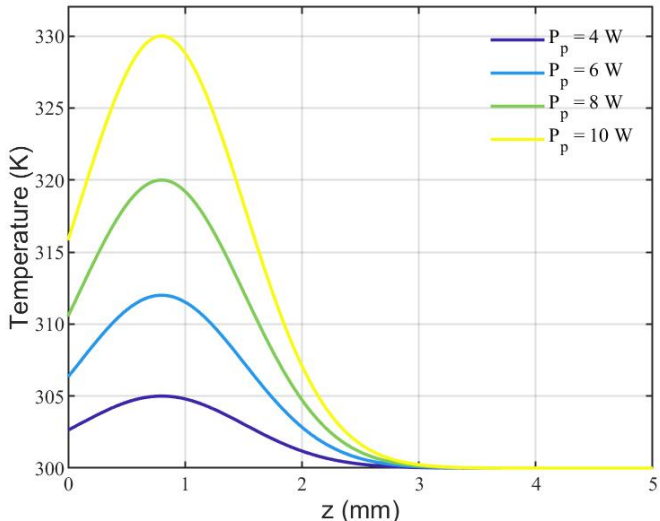


Figure 4 On-axis Temperature Distribution under Different Pump Powers

The non-uniform heat deposition directly induces an inhomogeneous temperature field within the crystal. As shown in the axial temperature distribution in Figure 4, the temperature profile along the optical axis closely resembles the heat source density curve, with the peak temperature also occurring at the pump end-face. This observation aligns with the fundamental principles of heat conduction theory. More importantly, the temperature exhibits a sharp increase with rising pump power. For instance, at Z=0, the maximum temperature under 10 W pumping is significantly higher than that under 4 W pumping, highlighting the critical thermal management challenges in high-power operation. However, the one-dimensional axial temperature distribution alone cannot fully capture the spatial complexity of thermal effects and their evolution with pump power. For the first time, Figure 5 presents the two-dimensional temperature field distribution across the crystal cross-section under pump powers ranging from 5 W to 20 W.

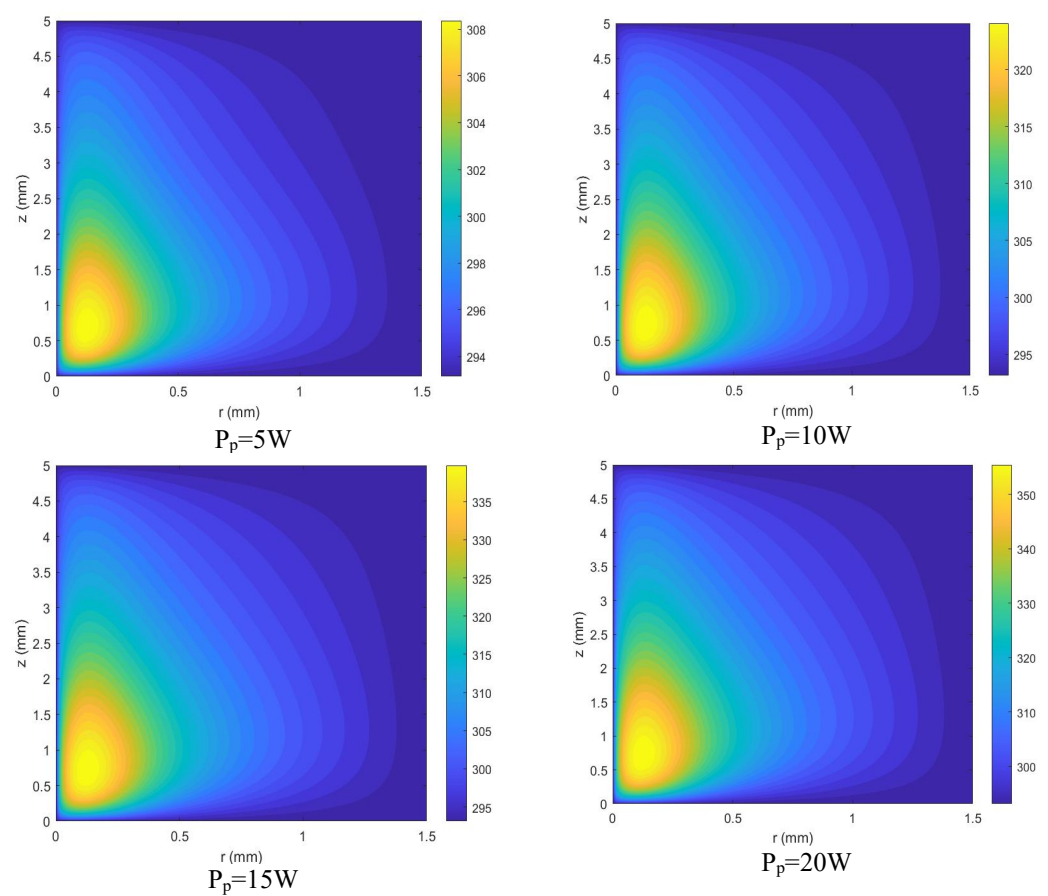


Figure 5 2D Temperature Field under Different Pump Powers

As observed from the temperature field distributions, the highest temperature region (hot spot) remains consistently localized at the center of the pump end-face across all pump powers, demonstrating clear spatial stability. As the pump power increases from 5 W to 20 W, the high-temperature zone expands significantly in both axial and radial directions, indicating rapid growth of the thermal-affected region with increasing power. Regarding temperature gradients, the elevated pump power not only raises the overall crystal temperature (consistent with the axial temperature profile in Figure 4) but also substantially intensifies the spatial temperature gradient across the crystal cross-section. Under 20 W pumping, the isotherms near the end-face center become notably denser compared to the 5 W condition, reflecting a sharp increase in the temperature variation per unit length. This enhanced gradient will inevitably lead to stronger thermal lensing effects and thermal stress. The observed evolution of the temperature field clearly demonstrates that core overheating and gradient intensification represent the primary thermal management challenges when scaling the laser power to 20 W, while also providing specific guidance and design boundaries for optimizing cooling structures under high-power conditions.

In summary, this section's simulation study reveals the complete chain of thermal effects in end-pumped crystals: pump light absorption creates an exponentially decaying heat source along the optical axis (Figure 3), which drives the formation of corresponding axial temperature gradients (Figure 4), ultimately manifesting as a strongly graded two-dimensional temperature field in the crystal cross-section (Figure 5)[13-16]. The severity of this temperature field increases substantially with rising pump power. These results systematically elucidate the formation and evolution mechanisms of thermal effects from fundamental principles to observable phenomena, providing crucial theoretical foundation for subsequent investigations of thermal lensing effects and laser output characteristics.

3.2 Influence of Pump Power and Spot Radius on Temperature Distribution

To further analyze the influence of pumping parameters on the temperature distribution within the Pr³⁺: YLF crystal, numerical simulations of the crystal temperature distribution were conducted under different pump powers and pump spot radii, based on the aforementioned thermal conduction model.

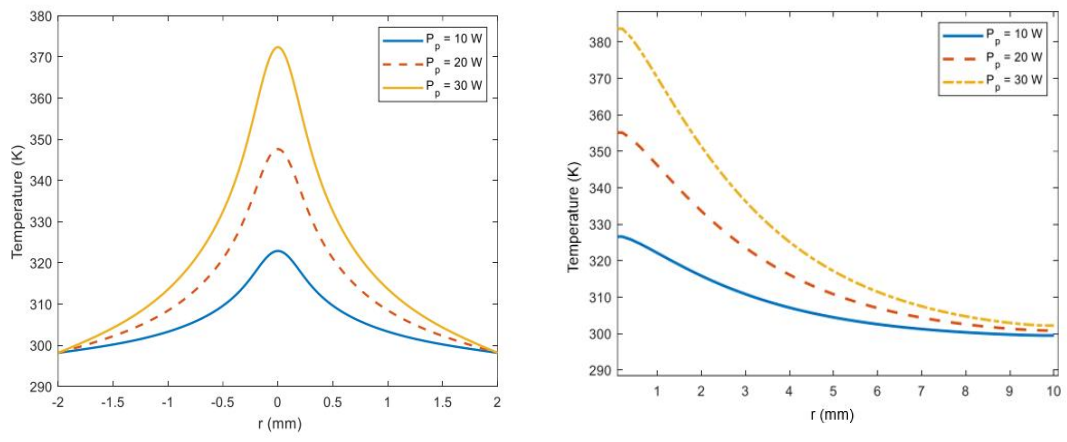


Figure 6 Steady-state Temperature Distribution of the Crystal End-face and Longitudinal Cross-section under Different Pump Powers

Figure 6 shows the steady-state temperature distributions at the crystal end-face (left) and longitudinal cross-section (right) under different pump powers (10 W, 20 W, and 30 W). It can be observed that as the pump power increases, heat deposition within the crystal is significantly enhanced, leading to greater non-uniformity in the temperature field. The highest temperature consistently occurs at the center of the pump end-face and decays gradually along the axial direction. When the pump power rises from 10 W to 30 W, the central temperature increases from approximately 322 K to 374 K, accompanied by a sharp rise in the overall temperature gradient. These results indicate that higher pump power induces stronger radial and axial thermal gradients, thereby intensifying thermal stress and thermal lensing effects.

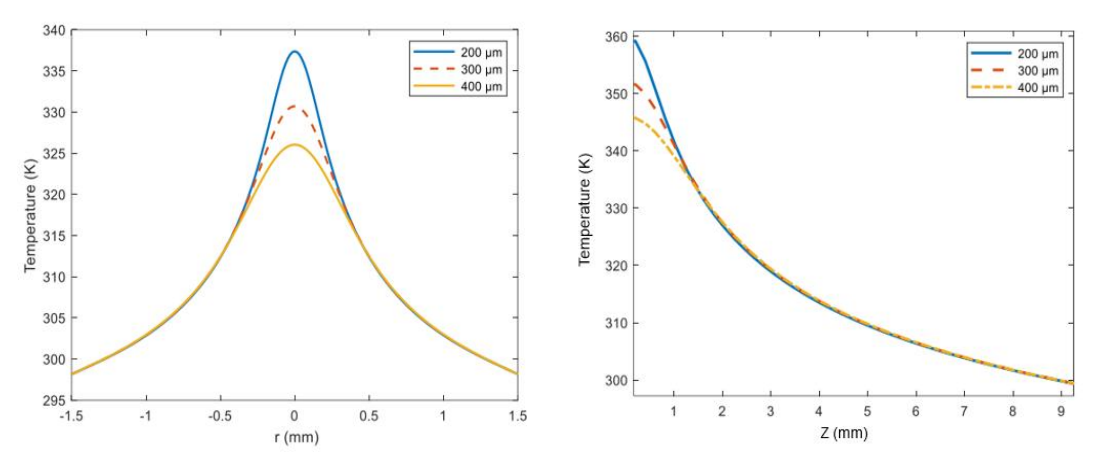


Figure 7 Temperature Distributions at Crystal end-face and Longitudinal Cross-section under Different Pump Spot Radii

Figure 7 presents the temperature distributions at the crystal end-face (left) and longitudinal cross-section (right) under different pump spot radii (200 μm, 300 μm, and 400 μm) at a fixed pump power of 10 W. As shown, the maximum temperature at the end-face gradually decreases with increasing spot radius. This behavior occurs because, at a constant pump power, a larger spot radius reduces the pump power density, thereby decreasing the heat deposition per unit volume. These results demonstrate that appropriately increasing the pump spot size can effectively reduce the axial temperature rise, improve heat dissipation, and mitigate thermal lensing distortion and thermal stress concentration. Therefore, both pump power and spot radius are critical parameters influencing the temperature distribution in Pr³+: YLF crystals. A higher pump power intensifies the thermal load effect, whereas a larger spot radius reduces the temperature rise and gradient[17-19]. Rational selection of these pumping parameters can effectively optimize the thermal management performance of the crystal, providing essential design guidelines for the stable operation of high-power end-pumped visible lasers.

3.3 Thermal Lensing Effect Analysis

In end-pumped laser configurations, Pr³⁺: YLF crystals generate non-uniform temperature fields upon absorbing pump radiation, resulting in radial temperature gradients. These gradients induce refractive index variations through the thermo-optic effect, forming a negative lens structure. Simultaneously, thermal stress further modifies the refractive index distribution via the photoelastic effect. The combined action of these mechanisms produces thermal lensing effects that significantly influence laser beam propagation characteristics. Table 1 summarizes the key parameters of

three Pr3+-doped laser crystals.

Table 1	Comparison	of Key Thermo	ophysical Parameters	s for Different Ci	rystal Materials

Crystal Materials	$K (\mathbf{W} \cdot \mathbf{m}^{-1})$	$ \frac{(dn / dT)}{(\times 10^{-6}/K)} $	α_T (×10 ⁻⁶ / K)	n	Characteristics Description
Pr ³⁺ :YLF	5.8	9.2	13.3	1.45	Anisotropic, moderate thermal conduction
Pr ³⁺ :YSO	3.4	10.8	7.2	1.80	Low conductivity, high heat accumulation
Pr ³⁺ :YAG	13.0	7.1	8.2	1.82	High conductivity, weakest lensing

As shown in the table, Pr³⁺: YAG crystal exhibits the highest thermal conductivity and the lowest thermal lensing sensitivity, resulting in smaller temperature gradients and weaker thermal lensing effects under identical pump power conditions. In contrast, Pr³⁺: YSO possesses the lowest thermal conductivity, hindering effective heat dissipation and leading to significant focal length reduction.

Figure 8 illustrates the thermal lens focal length characteristics of different crystal materials. As the pump power increases, all three crystals exhibit decreased focal lengths and enhanced thermal lensing effects. Among them, Pr^{3+} : YAG demonstrates the longest focal length and weakest thermal lensing, while Pr^{3+} : YSO shows the shortest focal length and strongest thermal lensing. Pr^{3+} : YLF exhibits intermediate performance with balanced thermal stability. The bar chart comparison at a fixed power of P = 10 W indicates that Pr^{3+} : YLF achieves an optimal balance between thermal effects and optical stability under high-power pumping conditions, making it a suitable gain medium for visible lasers.

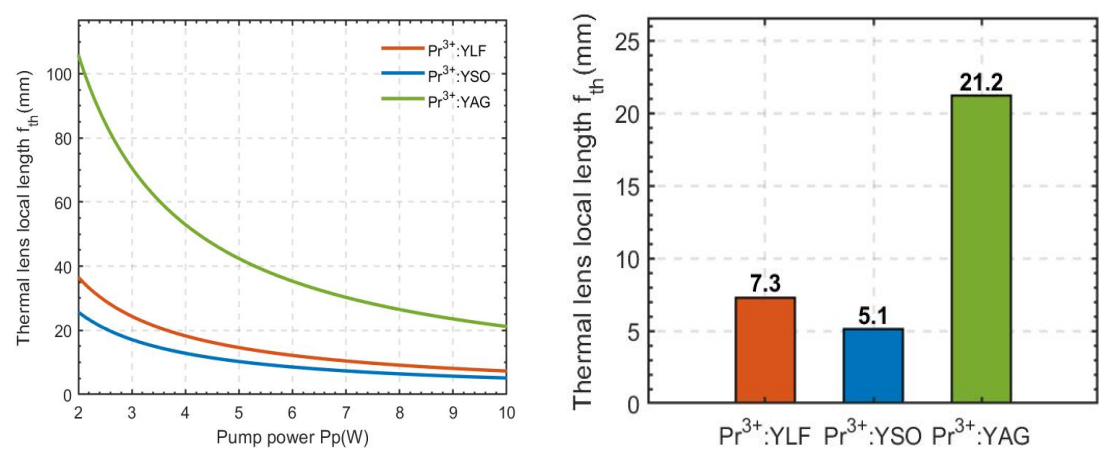


Figure 8 Material Comparison of Thermal Lensing Characteristics Versus Pump Power

In summary, the differences in thermophysical properties among crystal materials directly affect the strength of thermal lensing effects. For the design of high-power LD end-pumped visible lasers, crystals should be selected based on their thermal conductivity, thermo-optic coefficient, and thermal expansion characteristics to achieve optimal optical stability and thermal management performance.

To analyze the influence of pump power on the thermal lensing effect in the crystal, this study employs the equivalent focal length formula for thermal lenses. The analysis reveals that the thermal lens focal length is inversely proportional to the pump power. Specifically, as the pump power P_{abs} increases, the temperature rise within the crystal intensifies and the refractive index gradient steepens. This leads to a reduction in the thermal lens focal length, manifesting as enhanced beam divergence. The relationship is shown in Figure 9.

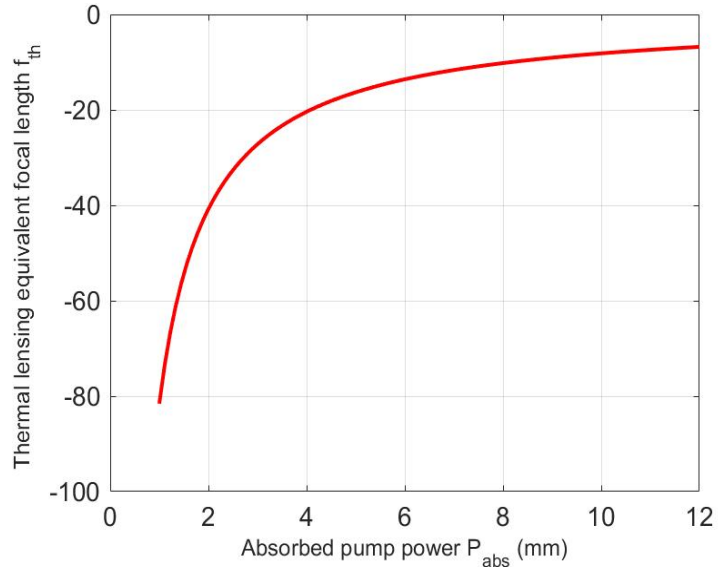


Figure 9 Thermal Lens Focal Length and Pump Power

As observed, the focal length decreases rapidly with increasing pump power, indicating enhanced thermal lensing effects. Without proper compensation, this will significantly degrade cavity stability and output beam quality. The focal length exhibits proportional dependence on the square of the beam radius and inverse proportionality to the absorbed power. The variation of thermal lens focal length under different pump spot radii further demonstrates that smaller spots yield shorter focal lengths and more pronounced thermal lensing. This occurs because, at constant power, smaller spot sizes generate higher thermal power density per unit area, leading to stronger refractive index gradients and consequently enhanced thermal lens divergence [20].

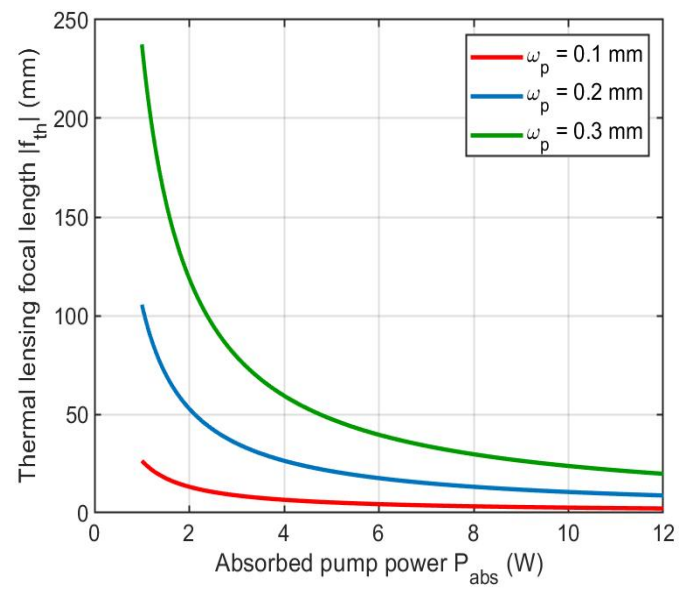


Figure 10 Thermal Lens Focal Length Versus Pump Spot Radius

As derived from the aforementioned thermal lensing formula, the pump spot radius is a critical parameter governing the strength of the thermal lensing effect. A smaller spot radius results in higher thermal power density, greater central temperature rise, and a steeper refractive index gradient, thereby intensifying the thermal lens. Conversely, a larger spot radius promotes more uniform heat distribution, leading to a weaker thermal lensing effect. Figure 10 illustrates the variation of thermal lens focal length with pump power for three different pump spot radii ω_p =0.1 mm,0.2 mm,0.3 mm. It can be observed that a higher pump power leads to a shorter focal length. However, the focal length exhibits a "nonlinear decrease" with increasing pump power, where the rate of decrease gradually diminishes. Under the same pump power condition , a smaller ω_p results in a shorter thermal lens focal length and a stronger thermal lensing effect[21]. This occurs because a smaller spot radius concentrates the thermal power density, leading to more pronounced refractive index changes. This trend highlights the significant influence of pump conditions on thermal effects and provides a theoretical basis for laser cavity design and stability optimization.

4 CONCLUSION

This study systematically investigates the thermal effects in LD end-pumped Pr³⁺: YLF green lasers through theoretical modeling, numerical simulation, and regular pattern analysis. The main conclusions are as follows:

- (1) The formation and evolution mechanism of the internal temperature field in the crystal has been revealed. The simulation results clearly demonstrate a complete causal chain: from "pump light absorption forming an exponentially decaying heat source" to "generating axial temperature gradients," and ultimately "forming a two-dimensional temperature field with strong spatial gradients." The pump end-face center consistently remains the core region of thermal effects, with both its influence range and gradient intensity significantly intensifying as power increases.
- (2) The regulatory effect of pump parameters on the thermal lensing was quantitatively characterized. The thermal lens focal length decreases nonlinearly with increasing pump power, showing an inverse relationship. Furthermore, the pump spot radius is identified as a critical parameter affecting the thermal lensing effect. Under identical pump power, a smaller spot radius concentrates the power density, resulting in a stronger thermal lensing effect.
- (3) The impact of crystal dimensions on thermal management was evaluated. The study reveals that increasing the crystal diameter effectively enhances heat dissipation capacity, reduces internal temperature rise and refractive index gradient, thereby yielding a longer thermal lens focal length and mitigating the thermal lensing effect. This finding provides guidance for optimizing thermal performance through crystal selection.

This research quantitatively elucidates the generation mechanisms and evolution patterns of thermal effects in Pr³⁺: YLF lasers. The findings provide clear guidance for thermal management design and resonator optimization in high-power, high-stability visible lasers.

COMPETING INTERESTS

The authors have no relevant financial or non-financial interests to disclose.

FUNDING

This work was supported by the Shaanxi Provincial Key Research and Development Program (Grant No. 2023-YBGY-016).

REFERENCES

- [1] Wang P, Yuan Q, Xia R, et al. Thermal effect analysis on cuboid Pr: YLF crystals pumped by blue laser diodes. Applied Optics, 2023, 62(18): 4797-4804.
- [2] Huang L, Xu X, Zhang N, et al. Recent advances for diode-pumped CW Pr:YLF lasers in visible region (Review). Optics and Laser Technology, 2024, 142, 105578. DOI: https://doi.org/10.1016/j.infrared.2024.105578.
- [3] Lin X, Feng Q, Zhu Y, et al. Diode-pumped wavelength-switchable visible Pr³⁺: YLF laser around 670 nm. Opto-Electronic Advances, 2021, 4(4): 210006. DOI: 10.29026/oea.2021.210006.
- [4] Tanaka H, Fujita S, Kannari F. High-power visibly emitting Pr3+: YLF laser end pumped by single-emitter or fiber-coupled GaN blue laser diodes. Applied optics, 2018, 57(21): 5923-5928.
- [5] Zhang L L. Research progress of blue LD-pumped rare-earth-doped visible fiber lasers. Chinese Journal of Lasers, 2022, 59(15): 1516016.
- [6] El-Agmy R M, Al-Hosiny N. Thermal analysis and experimental study of end-pumped Nd: YLF laser at 1053 nm. Optical Engineering, 2017, 56(9): 096104.
- [7] Chenais S, Druon F, Forget S, et al. On thermal effects in solid-state lasers: The case of ytterbium-doped materials. Progress in Quantum Electronics, 2006, 30(4): 89-153.
- [8] Chen S, Wang L M, Qiu H R. Thermal effect modeling and optimization of Pr³⁺: YLF crystal under high-power pumping. Laser & Optoelectronics Progress, 2023, 60(9): 091001.
- [9] Bruneau D, Delmonte S, Pelon J. Pump-to-mode size ratio dependence of thermal loading in diode-end-pumped solid-state lasers. Journal of Physics D: Applied Physics, 2007, 40(22): 6930-6938.
- [10] Hardman P J, Pollnau M, Clarkson W A, et al. Thermal lensing in high-power end-pumped Nd:YLF lasers. IEEE Journal of Quantum Electronics, 1997, 33(4): 599-606.
- [11] Peng X, Xu L, Asundi A. High-power efficient continuous-wave TEM_∞ intracavity frequency-doubled diode-pumped Nd: YLF laser. Applied Optics, 2005, 44(5): 800-807.
- [12] Liu Q, Wang L, Zhao C. Analysis of temperature field and thermal lens coupling characteristics in LD end-pumped solid-state lasers. Acta Photonica Sinica, 2024, 53(6): 0620001.
- [13] Ma S, Xiong Z, Liu Z, et al. Thermal effects and their suppression of end-pumped gradient-doped Nd:YAG crystals. Infrared Physics & Technology, 2025, 148, 105845. DOI: https://doi.org/10.1016/j.infrared.2025.105845.
- [14] Mironov E A, Kuznetsov I I, Palashov, O V, et al. Broadband amplification and thermal lensing in a Yb:YLF crystal in thin and thick geometries. Applied Optics, 2024, 63(14): 4508-4514.
- [15] Wang J Y, Pu S S, Wang X H, et al. 1.01-W narrow-linewidth ultraviolet laser by Pr: YLF. Optics and Laser Technology, 2024, 569, 130812. DOI: https://doi.org/10.1016/j.optcom.2024.130812.
- [16] Wang X, Liu J J, Li Q. Numerical analysis of thermal lensing effect in end-pumped Nd: YLF solid-state lasers. Acta Optica Sinica, 2022, 42(4): 0404001.
- [17] Lang B T, Song Y J, Zong N, et al. Anisotropic thermal and polarized spectroscopic properties of Nd: YLF crystal. Journal of Luminescence, 2024, 276, 120838. DOI: https://doi.org/10.1016/j.jlumin.2024.120838.

- [18] Kilinc M, Demirbas U, Gonzalez Diaz J B, et al. Thermal and population lensing of Yb:YLF at cryogenic temperatures. Optical Materials Express, 2023, 13(11): 3200-3212.
- [19] Jiang Z X, Li B X, Liao W B, et al. Performance study of blue weakly absorbed pumped Pr³⁺: YLF red laser. Chinese Journal of Lasers, 2024, 51(13): 1301003.
- [20] Davide Baiocco, Ignacio Lopez-Quintas, Javier R Vázquez de Aldana, et al. Thermal analysis of diode-pumped femtosecond-laser gain media. Optics & Laser Technology, 2025, 180, 111499. DOI: https://doi.org/10.1016/j.optlastec.2024.111499.
- [21] Eremeĭkin O N, Egorov N A, Zakharov N G, et al. Investigating a thermal lens in a Tm:YLF crystal under intense diode pumping. Journal of Optical Technology, 2009, 76(11): 676-679.